RSC Advances

ROYAL SOCIETY OF CHEMISTRY

www.rsc.org/advances

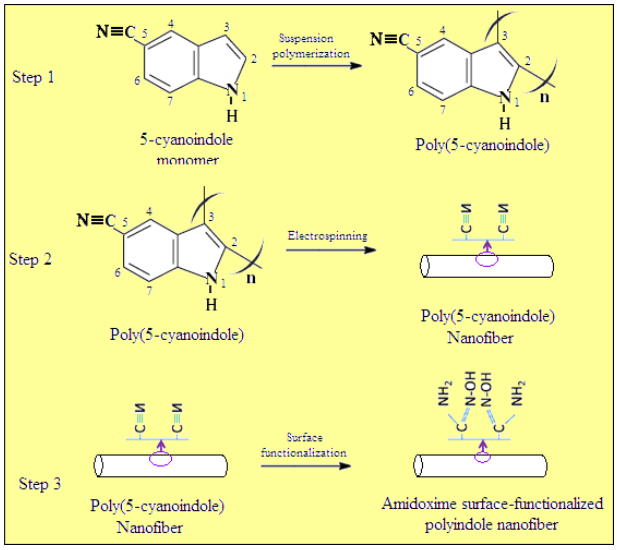

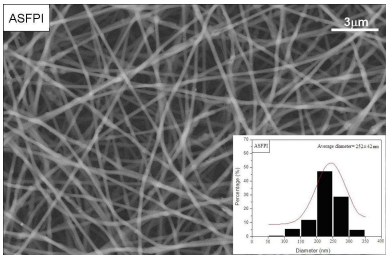

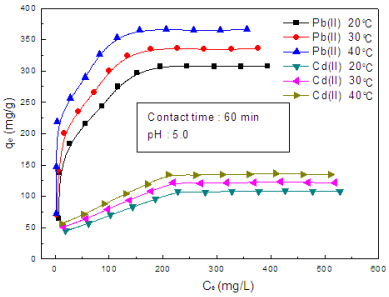

Preparation of amidoxime surface-functionalized polyindole (ASFPI) nanofibers for Pb(II) and Cd(II) Adsorption from Aqueous Solutions

Cai Zhijiang[1,2]*, Jia Jianru[1], Zhang Qing[1], Yang Haizheng[1]

1 School of Textiles, Tianjin Polytechnic University, Tianjin 300387, China,

2 State Key Laboratory of Hollow Fiber Membrane Materials and Processes, Tianjin 300387, China

No 399 BingShuiXi Street, XiQing District, Tianjin China, postcode 300387

Tel: 86-22-83955385

Fax: 86-22-83955187

*Corresponding Author: caizhijiang@hotmail.com

ABSTRACT

Amidoxime surface-functionalized polyindole (ASFPI) nanofibers were prepared by electrospinning of chemically synthesized poly(5-cyanoindole) followed by surface modification. The as-prepared ASFPI nanofibers were characterized with FTIR, SEM, BET surface areas and water contact angle measurement. Meanwhile, the adsorption properties and mechanism of ASFPI nanofibers towards Pb(II) and Cd(II) in aqueous solution were mainly investigated by batch method. It was found that ASFPI nanofibers showed high affinity towards Pb(II) and Cd(II). The maximum adsorption capacities were found to be 307.44 and 108.49 mg/g for Pb(II) and Cd(II), which are markedly high values compared to other fiber adsorbents reported. The adsorption isotherms were better fitted with the Langmuir model rather than Freundlich and Temkin models. The kinetics data analysis showed that the adsorption process could be described by pseudo-second order kinetic model, suggesting a chemisorption process as the rate limiting step. Thermodynamic parameters revealed the spontaneity of adsorption process and higher temperature favored adsorption. Regeneration tests showed that ASFPI nanofibers could be reused repetitively for 10 times with 80% of initial adsorption capacity.

Keywords: Poly(5-cyanoindole); Nanofiber; Surface-functionalization; Adsorption

1. Introduction

Water pollution by toxic heavy metals has become more and more serious with the rapid increase in global industrial activities. Various methods have been developed for the heavy metals removal such as solvent extraction, membrane separation, precipitation, reduction, electrochemical treatment, adsorption, flocculation, reverse osmosis and ion exchange [1-4]. Among these methods, adsorption is generally preferred due to its high efficiency, ease of handling and availability of different sorbents.

Nowadays, except various solid adsorbents such as activated carbon, oxide minerals, polymer materials, resins and biosorbents [5-8], conducting polymers have been proposed to be used for water treatment. They have shown good prospect for removing heavy metals from aqueous solution due to the presence of nitrogen atoms which can chelate metal ions through electrostatic [9]. For example, Olad and Kumar [10,11] have investigated the reduction of toxic Cr(VI) (62.9 mg/g) in aqueous solution using polyaniline as adsorbent. Ai [12] has prepared polyaniline nanosticks by ultrasonic-assisted method with Cu(II) uptake performance of 7.6 mg/g. Seid [13] has reported the removal of Cd(II) (71.4 mg/g) and Co(II) (70.04 mg/g) from aqueous solutions by polypyrrole particles. However, the adsorption capacities of these conducting polymer adsorbents are rather low. It is desirable to develop conducting polymer based adsorbents with higher removal capacity for practical application.

To approach this object, two methods can be adopted. One is to fabricate nano-sized fiber adsorbents with large surface areas and highly active surface sites by nanotechnology. Recently, polyaniline nanofibers and polyacrylonitrile/polypyrrole

core/shell nanofibers have been prepared as nano-adsorbents for the removal of Cr(VI) from aqueous solution [14,15]. Polypyrrole-coated electrospun nanofiber membranes have been reported for recovery of Au(III) from aqueous solution [16]. Polyaniline nanofibers assembled on alginate microsphere have been investigated for Cu(II) and Pb(II) uptake [17]. Another method is to chemically bond the chelating functional groups such as amino, carboxyl, sulfydryl and amidoxime onto the adsorbents surface [18,19,20]. Among these chelating groups, amidoxime group has a strong chelating ability towards a wide range of heavy metal ions such as UO_2(II), Cu(II), Pd(II), Cd(II) [21-24]. Therefore, it would be interesting to investigate the possibility of conducting polymer nanofibers with amidoxime surface functionalization for metal ions adsorption.

Polyindole is a conducting polymer, which possess the properties of both poly(para-phenylene) and polypyrrole together, such as fairly good thermal stability, high-redox activity, slow degradation rate in comparison with polyaniline and polypyrrole, and an air stable electrical conductivity [25-28]. In this study, amidoxime surface-functionalized polyindole (ASFPI) nanofibers were prepared by electrospinning of poly(5-cyanoindole) followed by surface modification. The ASFPI nanofibers were subsequently used for adsorption of Pd(II) and Cd(II) from aqueous solutions. The factors affecting adsorption properties such as pH value, metal ions concentration, contact time and temperature were investigated using batch method. The equilibrium data were analyzed using Langmuir, Freundlich and Temkin models. Kinetic and thermodynamic parameters of heavy metal ions adsorption were also calculated.

2. Experimental

2.1. Chemicals

5-cyanoindole, ammonium peroxydisulfate, hydroxylamine hydrochloride, sodium carbonate were purchased from Fluka Chemical Co., LTD and used as received. All other chemicals employed were of analytical reagent grade. Distillated water was used for all preparation and washing stages.

2.2 Preparation of poly(5-cyanoindole)

Poly(5-cyanoindole) was synthesized by suspension polymerization of 5-cyanoindole. 100 mL of chloroform were introduced into a 250 mL round-bottom flask, which was kept at 20 ℃ under nitrogen. 20 g of ammonium peroxydisulfate were then filled with 10 mL of water. 20 mL of chloroform and 3.2 g of 5-cyanoindole, using the reservoir with a tap, were then introduced in parallel into the flask in the course of 30 minutes. The molar ratio of ammonium peroxydisulfate to 5-cyanoindole was 4. The flask was then kept at 5 ℃ for 5 hours with stirring. The obtained product was filtered and washed with water and then dried under vacuum.

2.3 Electrospinning of poly(5-cyanoindole)

3 wt% solution was prepared by dissolving poly(5-cyanoindole) in acetonitrile under ultrasonification. The solution was then filled into a glass syringe terminated by a stainless steel needle with inner diameter of 0.40 mm. The syringe was placed in an automatic pump and solution was extruded out at a constant speed of 0.5 mL/h. A voltage of 25 kV was applied to the needle and the distance between the needle tip and collector was 20 cm. The electrospinning was done in an environmental chamber

with constant temperature at 25 ℃ and relative humidity of 35%.

2.4 Amidoxime surface-functionalization of polyindole (ASFPI)nanofibers

50 mL of 1.0 mol/L aqueous hydroxylamine hydrochloride solution and 50 mL of 1.0 mol/L aqueous sodium carbonate solution were mixed (pH=6.5). The mixed solution was added into a 250 mL beaker, followed by adding 0.5 g of electrospun poly(5-cyanoindole) (EPCI) nanofibers. The amidoximation transform reactions were carried out under N_2 atmosphere at 70 ℃ for 40 min. The cyano groups (−C≡N) on the surface of EPCI nanofibers reacted with hydroxylamine, leading to the formation of $-C(NH_2)=N-OH$ groups. After reaction, the obtained ASFPI nanofibers were thoroughly rinsed with water to remove the remaining salts, and dried at 50 ℃ under vacuum.

2.5 Characterization

The FTIR spectra were recorded using a Perkin Elmer Spectrum RX-I spectrophotometer with the KBr pellet technique. The ^1H NMR spectrum was recorded on a JEOL GAM-ECP600 NMR spectrometer and $CDCl_3$ was used as the solvent. The surface morphology was observed by scanning electron microscope (SEM, Model TM-3030). BET surface areas were measured by an automatic physisorption analyzer (Micromeritics Instruments). Water contact angle measurement was performed at 25 ℃ by pendant drop method, employing a contact-angle measurement apparatus (type DSA-10, made in KURSS Company, Germany).

2.6 Adsorption kinetics and equilibrium isotherm of metal ions onto ASFPI nanofibers

Experiments were performed with 0.1 g adsorbent in 250 mL Erlenmeyer flask with 150 mL of single-metal ion solution on a temperature controlled water bath shaker at 300 rpm. All experiments were carried out at 20 ℃ except the temperature experiments. The metal ions concentration in aqueous phase was determined using a Unicam atomic absorption spectrophotometer (AAS, model 939). The removal efficiency (*R%*) and the quantity of metal ions adsorbed per gram of adsorbent was calculated using Eq. (1) and (2).

$$R\% = \left(\frac{C_0 - C_e}{C_0} \right) * 100 \quad (1)$$

$$q_e = \left(\frac{C_0 - C_e}{m} \right) * V \quad (2)$$

where q_e (mg/g) is equilibrium sorption capacity, V (L) is the volume of metal ions solution, m (g) is the weight of dry adsorbent, C_o and C_e (mg/L) are the initial and equilibrium concentrations of metal ions, respectively.

The effect of pH on metal ions adsorption was studied by varying the pH value from 1.0 to 7.0 using 0.1 mol/L HCl and NaOH. The effect of metal ions concentration on adsorption was investigated in a concentration ranging from 50 to 600 mg/L. To investigate the effect of contact time on adsorption process, samples were withdrawn at different time intervals to determine the ions concentration and the equilibrium time. The isotherm studies were conducted at 20, 30, and 40 ℃ by varying ions concentration from 100 to 400 mg/L under the optimum pH.

2.7. Desorption and regeneration experiments

For desorption studies, 0.1 g ASFPI nanofibers mat was first contacted with 200mL 400mg/L Pb(II) and Cd(II) for 12 h at 20 optimum pH and ℃, respectively. Then the ASFPI nanofibers mat was rinsed with distilled water to remove any residual solution and was then dried at room condition for 24 h. After that the ASFPI nanofibers mat was immersed into 100 mL 2 ~ 10 mol/L HCl aqueous solutions and shaking at 20 ℃ for 1 h. The desorption efficiency (%) was calculated based on the percentage of the ratio between the desorbed and preadsorbed amounts of the ions. Chosen the best eluent determined by desorption efficiency and repeated above processes for ten times to estimate the regeneration performance.

3. Results and discussion

3.1 Preparation of ASFPI nanofibers

In this work, ASFPI nanofibers were prepared from 5-cyanoindole through subsequent steps as presented in Scheme 1. Firstly, poly(5-cyanoindole) was synthesized by suspension polymerization using ammonium peroxydisulfate as oxidants. Poly(5-cyanoindole) nanofibers were then fabricated via electrospinning technique. Finally, by the reaction with hydroxylamine which was librated from neutralization of hydroxylamine hydrochloride and sodium carbonate, the cyano groups on the surface of poly(5-cyanoindole) nanofibers were gradually converted into amidoxime groups (−C(NH_2)=N−OH), forming ASFPI nanofibers. The conversion of cyano groups (*C%*) and the content of the amidoxime groups (*AO*) can be determined by Eq. (3) and Eq. (4).

$$C\% = \left(\frac{W_1 - W_0}{W_0}\right) * \left(\frac{M_1}{M_0}\right) \times 100 \quad (3)$$

$$AO(mmol/g) = \left(\frac{W_1 - W_0}{W_0}\right) * \frac{1000}{M_0} \quad (4)$$

where W_0 and W_1 (g) denote the weights of the nanofibers before and after reaction, respectively. M_0 and M_1 (g/mol) are the molecular weight of hydroxylamine (33) and 5-cyanoindole (142). The conversion of cyano groups is about 21% and the content of *AO* on ASFPI nanofibers is about 1.5 mmol/g accordingly.

3.2 FT-IR study

Figure 1 shows the FTIR spectra of 5-cyanoindole monomer (a), poly(5-cyanoindole) (b), EPCI nanofibers (c) and ASFPI nanofibers (d). It is observed that the strong and broad band located around 3380 cm^{-1} characteristic to the N-H stretching vibrations occurs in curve (a) and (b). The band at 1504 cm^{-1} in curve (a) and (b) is assigned to the N-H deformations and also the vibration modes of C_2=C_3 aromatic bonds, typical of indole. These results imply the presence of N-H bonds on poly(5-cyanoindole) backbone. Thus, nitrogen atom is likely not the polymerization site. A sharp band around 2215 cm^{-1} can be observed in curve (a) and (b), which corresponds to the characteristic stretching vibrations of cyano group. A sharp peak at 741 cm^{-1} and the band at 1455 cm^{-1} observed in curve (a) and (b) are attributed to the characteristic out of plane deformations of the C-H bond in the benzene ring and stretching of benzene ring, respectively. These results suggest that the benzene ring is also not involved in the polymerization. A peak around 720 cm^{-1} in curve (a) is assigned to the characteristic feature of the in-phase vibrations of hydrogen species

ascribed to the C_2 and C_3 of 5-cyanoindole monomer. However, this band is found to be absent in curve (b). This result indicates that C_2 and C_3 of indole ring should be the possible sites of polymerization.

The spectra of EPCI nanofibers are same to poly(5-cyanoindole), which confirms the structural stability of poly(5-cyanoindole) during the electrospinning process. After amidoximation, the band of cyano group (C≡N) at 2215cm^{-1} almost disappears. There appear two new bands at 1640cm^{-1} and 950cm^{-1}. The former should be ascribed to the vibrations absorption of C=N bond in amidoxime group, and the latter should be attributed to the vibrations absorption of N-O bond in amidoxime group. From the FTIR spectra, the introduction of amidoxime groups on polyindole nanofibers can be confirmed.

3.3 ^1H NMR test

To further confirmation of the amidoxime groups on polyindole nanofibers, the ^1H NMR spectra of EPCI and ASFPI nanofibers were recorded and shown in Figure 2. In the spectrum of EPCI nanofibers, there are three groups of proton peaks. The peaks at 12.01, 12.07 and 12.58 ppm represent proton of N-H. The other three peaks between 9.1 and 9.4 ppm arise from the proton at 4-position of the benzene ring. Multiple of peaks attributed to the protons at 6 and 7-positions of benzene ring appear in region 7.8~7.9 ppm. All peaks in the ^1H NMR spectrum of EPCI are in agreement with the spectrum of poly(5-cyanoindole) [29]. In the ^1H NMR spectrum of ASFPI nanofibers, two new groups of proton peaks can be detected. The peaks appearing around 5.4 ppm and 8.7 ppm are assigned to $–NH_2$ and –OH protons. Comparison of the ^1H NMR

spectrum of EPCI nanofibers with ASFPI nanofibers clearly proves that C≡N groups on the EPCI converted successfully to amidoxime groups (−C(NH_2)=N−OH).

3.4 Characteristic of nanofibers

The SEM images and fiber diameter distributions of EPCI and ASFPI nanofibers are presented in Figure 3. EPCI nanofibers exhibit smooth surface, round shape and are randomly oriented. The average diameter and BET surface areas are about 234 ± 35 nm and 61.71 m^2g^{-1}, respectively. After amidoximation, the as-prepared ASFPI nanofibers become densely packed and the average diameter slightly increases to 252 ± 42nm. The reason might be attributed to the surface amidoxime groups, which can absorb water in air. No degradation or cracks appear on ASFPI nanofibers, which show almost same morphology to EPCI nanofibers.

The average diameter, BET surface areas and water contact angle of EPCI and ASFPI nanofibers are collected in Table 1. It is noteworthy that poly(5-cyanoindole) is hydrophobic while amidoxime is much more hydrophilic. Amidoximation of EPCI nanofibers result in the formation of −C(NH_2)=N−OH groups on the fibers surface, leading to considerable increase of hydrophilicity. The high hydrophilicity as well as large BET surface areas of ASFPI nanofibers favors metal ions uptake.

3.5 Adsorption behaviors

3.5.1 Effect of amidoximation on removal of metal ions

Surface functionalization can significantly improve the adsorption capacities of adsorbents. The effect of amidoxime surface-functionalization on metal ions removal was investigated using EPCI and ASFPI nanofibers as adsorbent and the results are

given in Figure 4. It is observed that the removal efficiency increases with an increase in adsorbent dose. This is due to an increase in the surface areas and availability of more active sites for sorption. The amounts of EPCI nanofibers required for the complete removal of Pb(II) and Cd(II) from their solutions are 70 and 120 mg, respectively. However, the amounts of ASFPI nanofibers required for the complete removal of Pb(II) and Cd(II) are 40 and 60 mg respectively. The adsorption capacity of the ASFPI nanofibers is therefore about 1.75-2.0 times (1.75 for Pb(II), 2.0 for Cd(II)) higher than that of EPCI nanofibers. The significant increase in metal ions adsorption capacity is attributed to the presence of amidoxime groups on ASFPI nanofibers. This result clearly indicates that amidoxime surface-functionalization can greatly improve the adsorption efficiency of polyindole nanofibers for metal ions.

3.5.2 Effect of pH and adsorption mechanism

Acidity is one of the key parameters in metal ions adsorption from aqueous solution. It not only affects the speciation of metal ions but also influences the ionization of functional groups on the surface of adsorbent. Figure 5 presents the effect of solution pH on Pb(II) and Cd(II) adsorption by ASFPI nanofibers. It can be observed that the Pb(II) and Cd(II) adsorption by ASFPI nanofibers is pH dependent. As pH < 5, the adsorption capacities increase with increasing pH value; as pH = 5, maximum adsorption capacities of 216.64 and 66.27 mg/g for Pb(II) and Cd(II) are achieved; as pH > 5, the adsorption capacities turn to decline with pH value increasing. The reason can be explained as following. At low pH, the nitrogen atom and amino groups of amidoxime on the surface of ASFPI nanofibers will lose the complex ability towards

metal ions due to high protonation (seen Eq. 5), leading to low adsorption capacity. With pH value increasing the degree of protonation of the nitrogen atom and amino groups gradually reduce. In addition, the dissociation degree of oxime-hydroxyl-groups increases and negative oxygen-ion of oxime-hydroxyl-groups can be produced (seen Eq. 6), which result in gradual increasement in adsorption capacity [22]. As pH > 5, the hydrolysis of metal ions becomes obvious which leads to the decline of the adsorption ability. Thus, all the following experiments are therefore performed at pH 5.

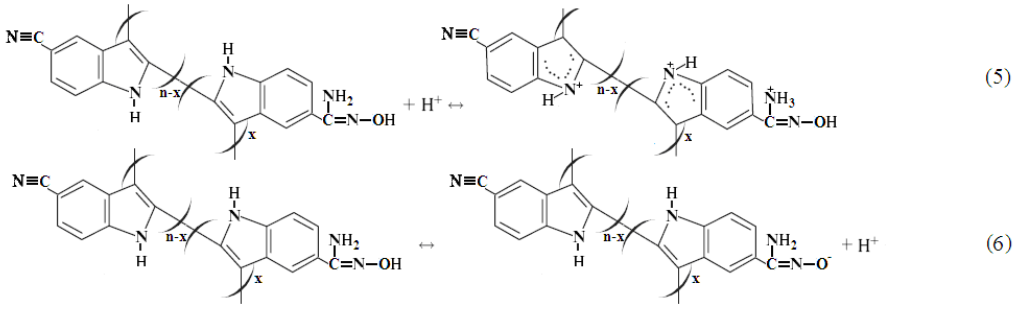

The adsorption action of ASFPI nanofibers for Pb(II) and Cd(II) should be a chemical sorption involving valence forces through sharing or exchange of electrons between adsorbent and adsorbate. The chelation of Pb(II) and Cd(II) onto ASFPI nanofibers can be explained with coordination between the electron-donating nature of O^- and N-containing groups on the surface of the fibers and electron-accepting nature of metal ions. Owing to the presence of two chelating components in ASFPI nanofibers, there are various possibilities for binding metal ions on the adsorbent. Scheme 2 presents possible adsorption mechanism of chelation of metal ions: chelation by the amidoxime groups (reaction I), chelation on the polyindole chains by the nitrogen atoms (reaction II), and chelation by the cooperation of amidoxime

groups and nitrogen atoms of polyindole chains (reaction III).

The adsorption capacity of ASFPI nanofibers for Pb(II) is much higher than Cd(II). The explanation for preferential sorption behavior is based on two facts. The first is that the hydrated ionic radius of Cd(II) is much bigger than that of Pb(II). The smaller metal ion (Pb(II)) has the higher adsorption capacity, which may be attributed to the fact that the smaller particles could reach easily to the active adsorption sites. We believe that there are some sterical hindrances, and therefore, ionic radii of the metal ions are playing important role in determining the adsorption capacity. The second reason is due to the relative stability of the complexes formed by Pb(II) and Cd(II) with amidoxime group. According to the Irring-Williams concept based on ligand field [30], the stability of metal cation-oxygen donor complexes decreases in the series: Pb(II) > Cd(II). The observed order of uptake for metal ions is the same as that of their increasing metals first hydrolysis constant. The logarithmic values of the metals first hydrolysis constant of the metal ions studied are as follows: $\log K_{Pb}$ = -7.71, $\log K_{Cd}$ = -10.08 [31]. Metal ions which form less soluble hydroxides are adsorbed more easily.

3.5.3 Effect of initial concentration and adsorption isotherm

Figure 6 shows the effect of initial metal ions concentration on equilibrium adsorption of ASFPI nanofibers. It is clear that the amount of metal ions adsorbed onto ASFPI nanofibers is increased with ions concentration increasing, and then reaches a plateau value. The equilibrium adsorption capacities increase from 65.26 to 307.44 mg/g for Pb(II) and 36.41 to 108.49 mg/g for Cd(II) when initial ions

concentration increases from 50 to 600 mg/L. In the case of low concentrations (< 400 mg/L for Pb, 300mg/L for Cd), the ratio of the available adsorption sites to the initial number of metal ions is larger and, subsequently, the fractional ion exchange becomes independent of initial concentrations. If the concentration is high (>400 mg/L for Pb, 300mg/L for Cd), ASFPI nanofibers could only achieve the saturation adsorption. This result shows that the removal of Pb(II) and Cd(II) by ASFPI nanofibers is highly concentration-dependent.

The adsorption isotherm of ASFPI nanofibers is investigated by Langmuir, Freundlich and Temkin models, respectively. The Langmuir model assumes that the uptake of metal ions occurs on a homogeneous surface by monolayer adsorption without any interaction between adsorbed ions. The Freundlich model assumes that the adsorption of metal ions occurs on a heterogeneous surface by monolayer adsorption. The Temkin model assumes that the heat of adsorption of the molecules decreases linearly due to sorbent−sorbate interactions. The Langmuir, Freundlich and Temkin model can be represented in the linearized form as:

$$\frac{C_e}{q_e} = \frac{1}{Q_m * K_L} + \frac{C_e}{Q_m} \quad (7)$$

$$\ln q_e = \ln K_F + \frac{\ln C_e}{n} \quad (8)$$

$$q_e = \frac{RT}{B_T} \ln K_T + \frac{RT}{B_T} \ln C_e \quad (9)$$

where Q_m (mg/g) is the maximum adsorption capacity, K_L (L/mg) is the Langmuir constant related to the energy of adsorption, K_F (mg/g) is the Freundlich constant related to the adsorption capacity and n is the heterogeneity factor, K_T (L/g) is the equilibrium binding constant corresponding to the maximum binding energy, B_T

(kJ/mol) is the Temkin constants related to the heat of adsorption, R (8.314J/mol/K) is the universal gas constant and T (K) is the absolute temperature.

The Langmuir, Freundlich and Temkin isotherm parameters for Pb(II) and Cd(II) adsorption by ASFPI nanofibers can be determined from the intercept and slope of the linear fitting line by plotting C_e *vs* C_e/q_e (Figure 7-A), $\ln q_e$ *vs* $\ln C_e$ (Figure 7-B) and q_e *vs* $\ln C_e$ (Figure 7-C). The obtained parameter values as well as the correlation coefficient (R^2) are summarized in Table 2. Comparison of R^2 values indicate that adsorption of Pb(II) and Cd(II) by ASFPI nanofibers is described better by Langmuir model (R^2 = 0.998 for Pb(II), 0.990 for Cd(II)) than Freundlich and Temkin models (R^2 = 0.833 for Pb(II), 0.924 for Cd(II) and R^2 = 0.943 for Pb(II), 0.915 for Cd(II)) at the studied temperature. The Q_m calculated by Langmuir model is 327.87 and 98.62 mg/g for Pb(II) and Cd(II), consistent with the actual saturated adsorption capacity (Pb(II) 307.44 mg/g, Cd(II) 108.49 mg/g) of ASFPI nanofibers, which also proves the monolayer adsorption is dominated.

Moreover, using Langmuir parameters, the dimensionless separation factor R_L could be calculated using Eq.10.

$$R_L = \frac{1}{1 + K_L C_0} \tag{10}$$

The variation of R_L with initial metal ions concentration is plotted in Figure 7-D. This factor can suggest the favorability of an adsorption process. R_L represents the adsorption process to be unfavorable ($R_L > 1$), linear ($R_L = 1$), favorable ($0 < R_L < 1$), or irreversible ($R_L = 0$). For all initial concentration studied, R_L values of Pb(II) and Cd(II) fall between 0 and 1, confirming the favorable nature of adsorption by the

ASFPI nanofibers. The R_L values decrease with initial concentration increasing, as shown in Figure 7-D. This result indicates that Pb(II) and Cd(II) adsorption is more favorable at higher initial concentration [32].

A comparison of the as-prepared ASFPI nanofibers with those of some other fiber adsorbents for the adsorption of Pb(II) and Cd(II) in recently reported literature is summarized in Table 3. As shown in Table 3, the maximum adsorption capacity of Pb(II) and Cd(II) by ASFPI nanofibers is comparable with that of other effective fiber adsorbents, and therefore ASFPI nanofibers could be recommended as an efficient alternative for the sorption of Pb(II) and Cd(II) from aqueous solution.

3.5.4 Effect of contacting time and Adsorption kinetics

Figure 8 displays the effect of contact time on the adsorption of metal ions by ASFPI nanofibers. It is evident that adsorption rate is fast in the initial stage of the process, then slows down markedly, and gradually reaches plateau. Equilibrium is attained within 30 and 45 min for Pb(II) and Cd(II), respectively. The half-load time ($t_{1/2}$) is less than 5 min for both metal ions. The high initial rate implies that the adsorption occurs essentially on the surface of ASFPI nanofibers. The adsorption rate of Pb(II) is higher than Cd(II) which might be due to higher affinity of the interacting amidoxime groups on the surface of ASFPI nanofibers.

In order to better understand the adsorption kinetic of Pb(II) and Cd(II) sorption onto ASFPI nanofibers, two commonly used kinetic models, namely, the Lagergren's pseudo-first-order and pseudo-second-order model are used. The pseudo-first-order model assumes diffusion is the rate limiting step of the adsorption process. On the

hand, pseudo-second-order model assumes chemisorption as the rate limiting step. The pseudo-first-order and the pseudo-second-order equations can be linearly expressed as follows:

$$\log(q_e - q_t) = \log q_e - \left(\frac{K_1}{2.303}\right)t \quad (11)$$

$$\frac{t}{q_t} = \frac{1}{K_2 q_e^2} + \left(\frac{1}{q_e}\right)t \quad (12)$$

where q_t (mg/g) is the adsorption capacity at time t (min), K_1 (1/min) is the pseudo-first-order rate constant, and K_2 (g/mg/min) is the pseudo-second-order rate constant. The kinetic parameters for pseudo-first-order and pseudo-second-order model are calculated from the intercept and slope of the linear fitting line by plotting $\log(q_e\text{-}q_t)$ *vs* t (Figure. 9a) and (t/q_t) *vs* t (Figure. 9b), respectively.

As seen from the results listed in Table 4, the pseudo-second-order model provides better correlation coefficients (R^2=0.995 for Pb(II) and 0.996 for Cd(II)) than the pseudo-first-order model (R^2=0.868 for Pb(II) and 0.888 for Cd(II)). Simultaneously, the good agreement between the calculated $q_{e,cal}$ values (299.40 mg/g for Pb(II), 95.60 mg/g for Cd(II)) and the experimental $q_{e,exp}$ values (307.44 mg/g for Pb(II), 108.49 mg/g for Cd(II)) suggests that the adsorption kinetic closely follows the pseudo-second-order model rather than the pseudo-first-order model. This indicates that the rate-limiting step may be chemisorption promoted by covalent/valence forces through exchange or sharing of electrons between adsorbent and adsorbate.

Furthermore, intra-particle diffusion model is also used to analyze the rate-limiting step in adsorption. The model can be expressed by the Weber-Morris equation as

following:

$$q_t = K_{ip} t^{0.5} + C \quad (13)$$

where K_{ip} (mg/g/min$^{0.5}$) is the intra-particle diffusion rate constant and the intercept C (mg/g) is constant related to the thickness of boundary layer. It is postulated that the intra-particle diffusion is considered to be the rate limiting step when the plot of q_t *vs* $t^{0.5}$ yields a straight line that passes through the origin.

The plot of q_t *vs* $t^{0.5}$ is given in Figure 9c. The adsorption plots of Pb(II) and Cd(II) do not pass through the origin suggesting that intra-particle diffusion is not the only rate limiting step. This behavior indicates that the Pb(II) and Cd(II) adsorption processes by ASFPI nanofibers involve more than one single kinetic stage. The initial rapid adsorption of metal ions may be governed by boundary layer diffusion and the subsequent slow uptake is attributed to the intra-particle diffusion effect [42]. The values of K_{ip} and C are obtained from the slope and intercept of the linear part of the plot of q_t *vs* $t^{0.5}$ (Fig. 9c) and listed in Table 4 along with the correction coefficients. The higher value of K_{ip} for Pb(II) obtained indicates that ASFPI nanofibers exhibit faster removal of Pb(II) from aqueous solutions.

3.5.5 Effect of temperature and adsorption thermodynamics

To investigate the effect of temperature on the adsorption of Pb(II) and Cd(II) by ASFPI nanofibers, adsorption experiments were carried out at three different temperatures (20, 30 and 40 ℃) and the results are shown in Figure 10. It can be seen that the adsorption capacities at equilibrium increase from 307.44 to 365.65 mg/g for Pb(II) and 108.49 to 134.58 mg/g for Cd(II) with temperature increasing from 20 to

40 ℃. As we known that the physical adsorption is an exothermic process, and the adsorption capacity always decreases with raising temperatures. It is apparent that the adsorption of Pb(II) and Cd(II) by ASFPI nanofibers is an endothermic process implying a chemical adsorption process [43]. This chemical adsorption is originated from the coordination and chelating action of the nitrogen atoms and amidoxime groups of ASFPI nanofibers towards Pb(II) and Cd(II) as we discussed before.

The thermodynamics parameters of Pb(II) and Cd(II) adsorption by ASFPI nanofibers, such as $\Delta G°$, $\Delta H°$ and $\Delta S°$ can be evaluated by the Van't Hoff equation (Eq. 14), which correlates $\Delta H°$ and $\Delta S°$ with Langmuir equilibrium constant, K_L.

$$\ln K_L = \frac{\Delta S^o}{R} + \frac{-\Delta H^o}{RT} \quad (14)$$

The slope, $\Delta H°/R$ and the intercept $\Delta S°/R$ obtained by plotting lnK_L *vs* $1/T$ (Figure 11) according to Eq.14 give $\Delta H°$ and $\Delta S°$ values, which are listed in Table 5. On the basis of the values of K_L as a function of temperatures, $\Delta G°$ values are calculated by Eq. 15 and listed in Table 5.

$$\Delta G^o = -RT \ln K_L \quad (15)$$

The positive values of $\Delta H°$ indicate that Pb(II) and Cd(II) adsorption by ASFPI nanofibers is an endothermic process. The positive values of $\Delta S°$ result from the increased randomness at the solid-solution interface due to the adsorption of metal ions. The negative values of $\Delta G°$ reveal that the adsorption process is spontaneous and thermodynamically favorable. The increase of the negative values of $\Delta G°$ with the increase of temperature suggests an increased trend in the degree of spontaneity of the metal ions sorption. The thermodynamics parameters of ASFPI nanofibers for Pb(II)

and Cd(II) adsorption imply chemisorption rather than physisorption, which are fitted to the deduction obtained from the adsorption kinetics.

3.6 Desorption and Reusability

For the potential application of ASFPI nanofibers in industrial wastewater treatment, reusability is very important. The desorption behavior of ASFPI nanofibers is graphically shown in Figure 12. It is found that increasing the HCl concentration results in a monotonous increase in the desorbed amounts of the metal ions. Based on the obtained results, the desorption efficiency of over 90% (93% for Pb(II) and 91% for Cd(II)) could be achieved with the use of 6 mol/L HCl solution as the desorbing solution. After desorption, repeated adsorption/desorption cycles are performed to examine the reusability of the ASFPI nanofibers and the results are shown in Figure 13. It could be found out that the ASFPI nanofibers have good reusability performance. After ten cycles, the adsorption capacities remain 255.18 mg/g for Pb(II) and 86.79 mg/g for Cd(II), which are about 83% and 80% of the new ASFPI nanofibers.

4. Conclusion

By using a three-step process, suspension polymerization of 5-cyanoindole, electrospinning of poly(5-cyanoindole) and surface-functionalization of EPCI nanofibers, ASFPI nanofibers were successfully prepared. Amidoxime surface-fuctionalization can greatly improve the metal ions adsorption efficiency. The maximum adsorption capacities of ASFPI nanofibers follow the order Pb(II) > Cd(II). The reason can be explained in terms of the hydrated ionic radius and relative stability

of the complexes. The experimental data fit well with Langmuir isotherm equation and pseudo-second-order kinetic model, which indicate that the chemisorption is the controlling mechanism and the monolayer adsorption is dominated. The adsorption process is spontaneous and endothermic. ASFPI nanofibers could be reused repetitively for 10 times with more than 80% of initial adsorption capacity. These results strongly suggest that ASFPI nanofibers have promising potential as an adsorbent for the removal of heavy metal ions from aqueous solutions and industry wastewaters.

Reference

[1] H. Bessbousse, T. Rhlalou, J.-F. Verchère, L. Lebrun, Removal of heavy metal ions from aqueous solutions by filtration with a novel complexing membrane containing poly(ethyleneimine) in a poly(vinyl alcohol) matrix, J Membrane Sci. 307 (2008) 249–259.

[2] C.P. Barbosa, G.R.P. Malpass, D.W. Douglas, L. Gomes, Electrochemical Removal of Cu(II) in the Presence of Humic Acid, J Brazil Chem Soc. 4 (2010) 651–658.

[3] A. da Browski, Z. Hubicki, P.P._Scielny, E. Robens, Selective removal of the heavy metal ions from waters and industrial wastewaters by ion-exchange method, Chemosphere. 56 (2004) 91–106

[4] N. Li, R. Bai, Development of chitosan-based granular adsorbents for enhanced and selective adsorption performance in heavy metal removal, Water Sci Technol. 54 (2006) 103–113.

[5] B.E. Reed，S.K. Nonavinakere, Metal Adsorption by Activated Carbon: Effect of Complexing Ligands, Competing Adsorbates, Ionic Strength, and Background

Electrolyte, Sep Sci Technol. 27 (1992) 1985–2000.

[6] J.E. van Benschoten, B.E Reed, M.R. Matsumoto, P. J. McGarvey, Metal removal by soil washing for an iron oxide coated sandy soil, Water Environ Res. 66 (1994) 168–174.

[7] B. Li, F. Su, H.-K. Luo, L. Liang, B. Tan, Hypercrosslinked microporous polymer networks for effective removal of toxic metal ions from water, Micropor Mesopor Mat. 138 (2011) 207–214.

[8] U. Farooq, J.A. Kozinski, M.A. Khan, M. Athar, Biosorption of heavy metal ions using wheat based biosorbents-A review of the recent literature, Bioresource Technol. 101 (2010) 5043–5053.

[9] R. Ansari, Application of Polyaniline and its Composites for Adsorption/Recovery of Chromium (VI) from Aqueous Solutions, Acta Chim Slov. 53 (2006) 88–94.

[10] A. Olada, R. Nabavi, Application of polyaniline for the reduction of toxic Cr(VI) in water, J Hazard Mater. 147 (2007) 845–851.

[11] P.A. Kumar, S. Chakraborty, M. Ray, Removal and recovery of chromium from wastewater using short chain polyaniline synthesized on jute fiber, Chem Eng J. 141 (2008) 130–140.

[12] L. Ai, J. Jiang, Ultrasonic-assisted synthesis of polyaniline nanosticks, and heavy metal uptake performance, Mater Lett. 65 (2011) 1215–1217.

[13] L. Seid, D. Chouder, N. Maouche, I. Bakas, N. Barka, Removal of Cd(II) and Co(II) ions from aqueous solutions by polypyrrole particles: Kinetics, equilibrium and thermodynamics, J Taiwan Inst Chem E. 45 (2014) 2969–2974.

[14] X. Guo, G.T. Fei, H. Su, L.D. Zhang, High-performance and reproducible polyaniline nanowire/tubes for removal of Cr(VI) in aqueous solution, J Phys Chem C. 115 (2011) 1608–1613.

[15] J. Wang, K. Pan, Q. He, B. Cao, Polyacrylonitrile/polypyrrole core/shell nanofiber mat for the removal of hexavalent chromium from aqueous solution, J Hazard Mater. 244-245 (2013) 121–129.

[16] H. Wang, J. Ding, B. Lee, X. Wang, T. Lin, Polypyrrole-coated electrospun nanofibre membranes for recovery of Au(III) from aqueous solution, J Membrane Sci. 303 (2007) 119–125.

[17] N. Jiang, Y. Xu, Y. Dai, W. Luo, L. Dai, Polyaniline nanofibers assembled on alginate microsphere for Cu^{2+} and Pb^{2+} uptake, J Hazard Mater. 215-216 (2012) 17–24.

[18] S.-H. Huang, D.-H. Chen, Rapid removal of heavy metal cations and anions from aqueous solutions by an amino-functionalized magnetic nano-adsorbent, J Hazard Mater. 163 (2009) 174–179.

[19] C.K. Ahn, D. Park, S.H. Woo, J.M. Park, Removal of cationic heavy metal from aqueous solution by activated carbon impregnated with anionic surfactants. J Hazard Mater. 164 (2008) 1130–1136.

[20] R. Coskun, C. Soykan, Preparation of amidoximated polyester fiber and competitive adsorption of some heavy metal ions from aqueous solution onto this fiber, J Appl Polym Sci. 112 (2009) 1798–1807.

[21] D.D. Diogo, M.H. Herbst, R. Ribeiro, V.G. Teixeira, The role of matrix porosity in the adsorption of Cu(II) by amidoxime chelating resins: An electron paramagnetic resonance study, React Funct Polym. 71 (2011) 721–727.

[22] B. Gao, Y. Gao, Y. L, Preparation and chelation adsorption property of composite chelating material poly(amidoxime)/SiO_2 towards heavy metal ions, Chem Eng J. 158 (2010) 542–549.

[23] A.F. Shaaban, D.A. Fadel, A.A. Mahmoud, M.A. Elkomy, S.M. Elbahy,

Synthesis of a new chelating resin bearing amidoxime group for adsorption of Cu(II), Ni(II) and Pb(II) by batch and fixed-bed column methods, J Environ Chem Eng. 2 (2014) 632–641.

[24] A. Zhang, T. Asakura, G. Uchiyama, The adsorption mechanism of uranium(VI) from seawater on a macroporous fibrous polymeric adsorbent containing amidoxime chelating functional group, React Funct Polym. 57 (2003) 67–76.

[25] D. Billaud, E.B. Maarouf, E. Hannecart, Chemical oxidation and polymerization of indole, Synth Met. 69 (1995) 571–572.

[26] E.B. Maarouf, D. Billaud, E. Hannecart, Electrochemical cycling and electrochromic properties of polyindole, Mater Res Bull. 29 (1994) 637–643.

[27] P.S. Abthagir, K. Dhanalakshmi, R. Saraswathi, Thermal studies on polyindole and polycarbazole, Synth Met. 93 (1998) 1–7.

[28] R. Lazzaroni, A.D. Pryck, C.H. Debraisieux, J. Riga, J. Verbist, J.L. Brédas, J. Delhalle, J.M. André, Electronic structure of conducting polymers from heteroaromatic bicyclic compounds, Synth Met. 21 (1987) 189–195.

[29] Z. Cai, J. Guo, H. Yang, Y. Xu, Electrochemical properties of electrospun poly(5-cyanoindole) submicron-fibrous electrode for zinc/polymer secondary battery, J Power Sources 279 (2015) 114–122.

[30] F.A. Cotton, G. Wilkinsons, C.A. Murillo, M. Bochmann, Advanced Inorganic Chemistry, third ed., Wiley-Interscience, New York, 1995.

[31] M.C. Newman, J.T. Mccloskey, Predicting Relative Toxicity and Interactions of Divalent Metal Ions: Microtox Bioluminescence Assay, Environ Toxicol Chem. 15 (1996) 275–281.

[32] W. Shen, Sh. Chen, Sh. Shi, X. Li, X. Zhang, W. Hu, H. Wang, Adsorption of Cu(II) and Pb(II) onto diethylenetriamine-baterial cellulose, Carbohyd Polym. 75

(2009) 110–114.

[33] G. Zhang, R. Qu, C.i Sun, C. Ji, H. Chen, C. Wang, Y. Niu, Adsorption for Metal Ions of Chitosan Coated Cotton Fiber, J Appl Polym Sci. 110 (2008) 2321–2327.

[34] C. Duan, N. Zhao, X. Yu, X. Zhang, J. Xu, Chemically modified kapok fiber for fast adsorption of Pb^{2+}, Cd^{2+}, Cu^{2+} from aqueous solution, Cellulose. 20 (2013) 849–860.

[35] R. Coskun, C. Soykan, Preparation of Amidoximated Polyester Fiber and Competitive Adsorption of Some Heavy Metal Ions from Aqueous Solution onto This Fiber, J Appl Polym Sci. 112 (2009) 1798–1807.

[36] P. Zou, Y. Guo, Y. Li, Adsorption of Pb(□) and Cd(□) from Contaminated Water by Activated Carbon Fiber, Environ Sci Technol China. 35 (2012) 49–53.

[37] M. Stephen, N. Catherine, M. Brenda, K. Andrew, P. Leslie, G. Corrine, Oxolane-2,5-dione modified electrospun cellulose nanofibers for heavy metals adsorption, J Hazard Mater. 192 (2011) 922–927.

[38] J. Xiong, C. Jiao, C. Li, D. Zhang, H. Lin, Y. Chen, A versatile amphiprotic cotton fiber for the removal of dyes and metal ions, Cellulose. 21 (2014) 3073–3087.

[39] S. Wang, L. Wang, W. Kong, J. Ren, C. Liu, K. Wang, R. Sun, D. She, Preparation, characterization of carboxylated bamboo fibers and their adsorption for lead(II) ions in aqueous solution, Cellulose. 20 (2013) 2091–2100.

[40] Y. Tian, M. Wu, R. Liu, Y. Li, D. Wang, J. Tan, R. Wu, Y. Huang, Electrospun membrane of cellulose acetate for heavy metal ion adsorption in water treatment, Carbohyd Polym. 83 (2011) 743–748.

[41] P. Kampalanonwat, P. Supaphol, Preparation and Adsorption Behavior of Aminated Electrospun Polyacrylonitrile Nanofiber Mats for Heavy Metal Ion Removal, Appl Mater Interfaces. 2 (2010) 3619–3627.

[42] J.C. Igwe, A.A. Abia, C.A. Ibeh, Adsorption kinetics and intraparticulate diffusivities of Hg, As and Pb ions on unmodified and thiolated coconut fiber, Int J Environ Sci Tech. 5(2008) 83-92.

[43] M.E. Argun, S. Dursun, M. Karatas, M. Guru, Activation of pine cone using Fenton oxidation for Cd(II) and Pb(II) removal, Bioresource Technol. 99 (2009) 8691–8698.

Nomenclature

q_e equilibrium sorption capacity (mg/g)

q_t adsorption capacity at time t (mg/g)

V solution volume (L)

m the amount of added adsorbent (g)

M the molecular weight (g/mole)

W the weight (g)

C_o initial Pb(II) concentrations (mg/L)

C_e equilibrium Pb(II) concentrations (mg/L)

Q_m maximum adsorption capacity (mg/g)

K_L the Langmuir constant (L/mg)

K_F the Freundlich constant (mg/g)

n the heterogeneity factor

K_T the equilibrium binding constant (L/g)

B_T the Temkin constant (KJ/mole)

R^2 correlation coefficient

R the universal gas constant (8.314 J/(K mole))

T the absolute temperature (K)

R_L the dimensionless separation factor

K_1 the pseudo-first-order rate constant (1/min)

K_2 the pseudo-second-order rate constant (g/(mg min))

K_{ip} the intra-particle diffusion rate constant (mg/g/min$^{0.5}$)

C constant related to the thickness of boundary layer (mg/g)

$\Delta G°$ standard Gibbs free energy change (KJ/mole)

$\Delta H°$ enthalpy change (KJ/mole)

$\Delta S°$ entropy change (KJ/mole)

Captions of Tables and Figures

Table 1 The Characteristics of EPCI and ASFPI nanofibers

Table 2 Langmuir, Freundlich and Temkin isotherm parameters for Pb(II) and Cd(II) adsorption by ASFPI nanofibers

Table 3 Comparison of the adsorption capacity of ASFPI nanofibers with those of

some other fiber adsorbents reported in literature for the adsorption of Pb(II) and Cd(II)

Table 4 Kinetic parameters for Pb(II) and Cd(II) adsorption by ASFPI nanofibers

Table 5 Thermodynamic parameters for Pb(II) and Cd(II) adsorption by ASFPI nanofibers

Scheme 1 Schematic illustration of preparation process of ASFPI nanofibers

Scheme 2 Possible adsorption mechanisms of ASFPI nanofibers for Pb(II) and Cd(II)

Figure 1 FTIR spectra of 5-cyanoindole monomer (a), poly(5-cyanoindole) (b), EPCI nanofibers (c) and ASFPI nanofibers (d)

Figure 2 ^{1}H NMR spectra of the EPCI (a) and ASFPI (b) nanofibers

Figure 3 SEM images and fiber diameter distribution of EPCI and ASFPI nanofibers

Figure 4 Effect of adsorbent dose on the removal efficiency of Pb(II) and Cd(II) by EPCI and ASFPI nanofibers

Figure 5 The effect of solution pH on Pb(II) and Cd(II) adsorption by ASFPI nanofibers

Figure 6 The effect of initial ions concentration on Pb(II) and Cd(II) adsorption by ASFPI nanofibers

Figure 7 Sorption isotherm displayed in their linearized format and fit by the Langmuir model (A), Freundlich model (B) and Temkin model (C) and the variation of R_L with initial concentration of metal ions (D)

Figure 8 The effect of contact time on Pb(II) and Cd(II) adsorption by ASFPI nanofibers

Figure 9 Data fitting for Pb(II) and Cd(II) adsorption by ASFPI nanofibers using pseudo-first-order kinetic model (a), pseudo-second-order kinetic model (b) and intra-particle diffusion model (c)

Figure 10 The effect of temperature on Pb(II) and Cd(II) adsorption by ASFPI nanofibers

Figure 11 Plot to determine thermodynamic parameters for Pb(II) and Cd(II) adsorption by ASFPI nanofibers

Figure 12 Desorption of Pb(II) and Cd(II) from the metal-loaded ASFPI nanofibers in HCl solution

Figure 13 Adsorption capacities of ASFPI nanofibers after regeneration

Table 1 The Characteristics of EPCI and ASFPI nanofibers

Nanofibers	Average Diameter (nm)	BET surface areas (m^2g^{-1})	Water contact angle (º)
EPCI	234 ± 35	61.71	124
ASFPI	252 ± 42	59.36	76

Table 2 Langmuir, Freundlich and Temkin isotherm parameters for Pb(II) and Cd(II) adsorption by ASFPI nanofibers

Metal	Langmuir model			Freundlich model			Temkin model		
ions	Q_m (mg/g)	K_L(L/mg)	R^2	K_F(mg/g)	n	R^2	K_T(L/g)	B_T(kJ/mol)	R^2
Pb	327.87	0.0466	0.998	56.98	3.24	0.833	120.25	0.143	0.943
Cd	98.62	0.0159	0.990	12.77	3.12	0.924	539.47	0.0513	0.915

Table 3 Comparison of the adsorption capacity of ASFPI nanofibers with those of some other fiber adsorbents reported in literature for the adsorption of Pb(II) and Cd(II)

Adsorbents	Metal ions	Operating conditions	Adsorption capacity	Ref
Chitosan Coated Cotton Fiber	Pb(II) Cd(II)	1 mmol/L pH 6.5	101.65 mg/g 15.76 mg/g	33
Diethylenetriamine pentaacetic acid modified Kapok fiber	Pb(II) Cd(II)	400 mg/L pH 5.5	310.6 mg/g 163.7 mg/g	34
Amidoximated Polyester Fiber	Pb(II) Cd(II)	130 mg/L pH 6	66.84 mg/g 13.11 mg/g	35
Activated Carbon Fiber	Pb(II) Cd(II)	100 mg/L pH 5.6	232.4 mg/g 33.8 mg/g	36
Electrospun cellulose nanofibers modified with oxolane-2,5-dione	Pb(II) Cd(II)	100 mg/L pH 6	250.47 mg/g 66.32 mg/g	37
Amphiprotic cotton fiber	Pb(II)	400 mg/L pH 6	70.6 mg/g	38
Carboxylated bamboo fibers	Pb(II)	100 mg/L pH 5.6	127.1 mg/g	39
PAA modified electrospun cellulose acetate nanofiber membranes	Cd(II)	30 mg/L pH 6	3.04 mg/g	40
Aminated electrospun polyacrylonitrile nanofiber Mats	Pb(II)	40 mg/L pH 4	60.6 mg/g	41
Polyaniline nanofibers assembled on calcium alginate microsphere	Pb(II)	10 mg/L pH 7	251.25mg/g	17
Amidoxime surface-functionalized polyindole (ASFPI) nanofibers	Pb(II) Cd(II)	400 mg/L pH 5	307.44 mg/g 108.49 mg/g	This study

Table 4 Kinetic parameters for Pb(II) and Cd(II) adsorption by ASFPI nanofibers

Ions	$q_{e,exp}$ (mg/g)	Pseudo-first-order model			Pseudo-second-order model			Intra-particle diffusion model		
		K_1 (1/min)	$q_{e,cal}$ (mg/g)	R^2	K_2 (g/mg/min)	$q_{e,cal}$ (mg/g)	R^2	K_{ip} (mg/g/min$^{0.5}$)	C (mg/g)	R^2
Pb(II)	307.44	0.0952	206.19	0.868	0.000565	299.40	0.995	48.41	5.81	0.958
Cd(II)	108.49	0.180	79.73	0.888	0.00142	95.60	0.996	13.68	2.52	0.965

Table 5 Thermodynamic parameters for Pb(II) and Cd(II) adsorption by ASFPI nanofibers

Metal ions	$\Delta G°$（kJ/mol）			$\Delta H°$	$\Delta S°$	R^2
	293K	303K	313K	(kJ/mol)	(J/mol·K)	
Pb(II)	-9.36	-10.40	-11.70	36.53	156.40	0.986
Cd(II)	-6.74	-7.43	-7.71	8.49	40.15	0.994

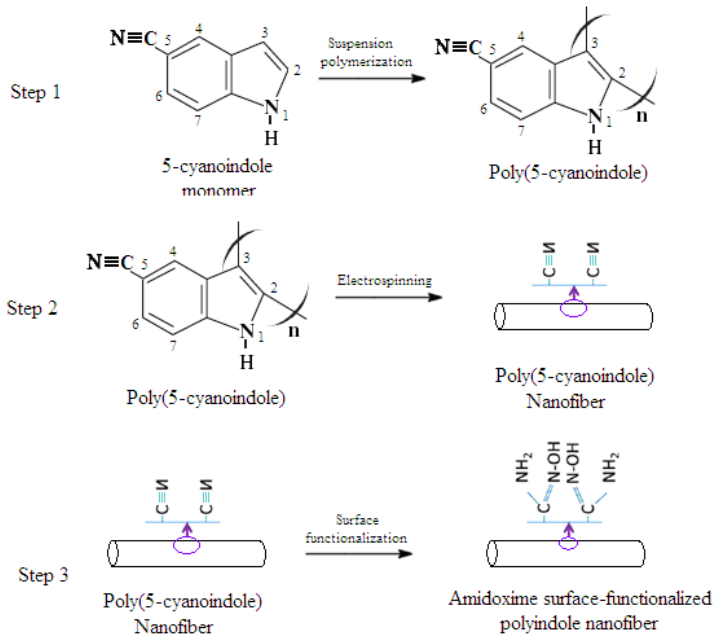

Scheme 1 Schematic illustration of preparation process of ASFPI nanofibers

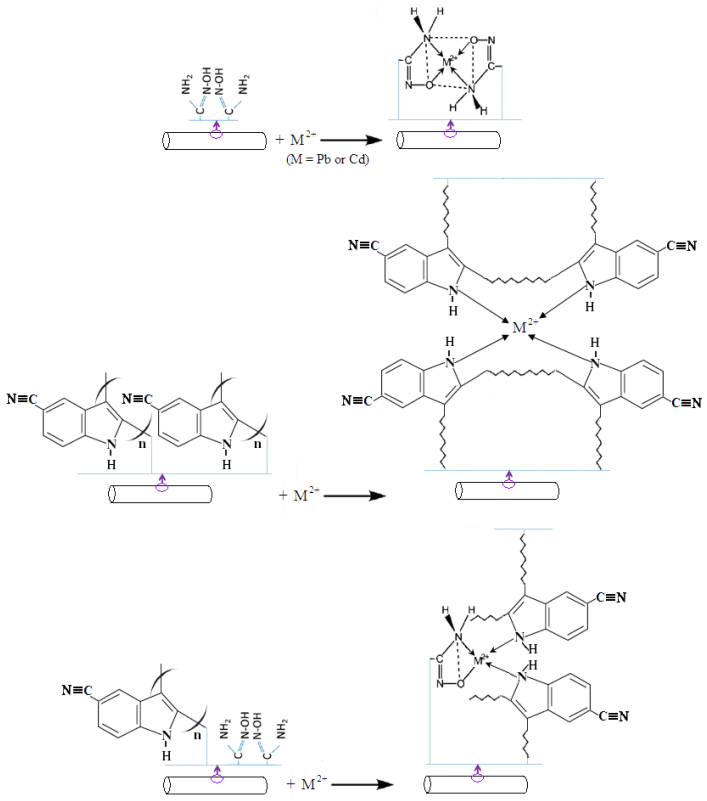

Scheme 2 Possible adsorption mechanisms of ASFPI nanofibers for Pb(II) and Cd(II)

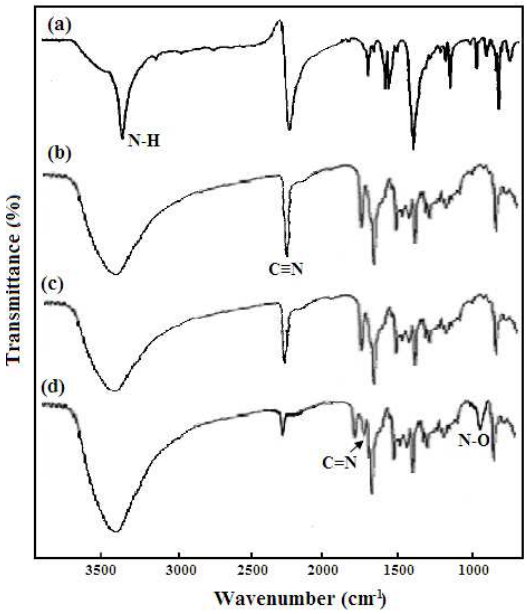

Figure 1 FTIR spectra of 5-cyanoindole monomer (a), poly(5-cyanoindole) (b), EPCI nanofibers (c) and ASFPI nanofibers (d)

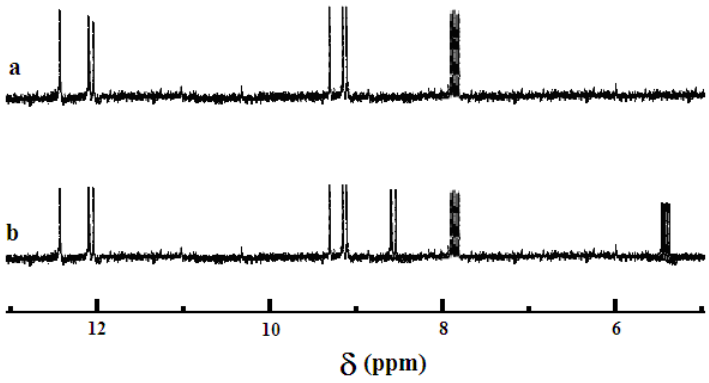

Figure 2 ^{1}H NMR spectra of the EPCI (a) and ASFPI (b) nanofibers

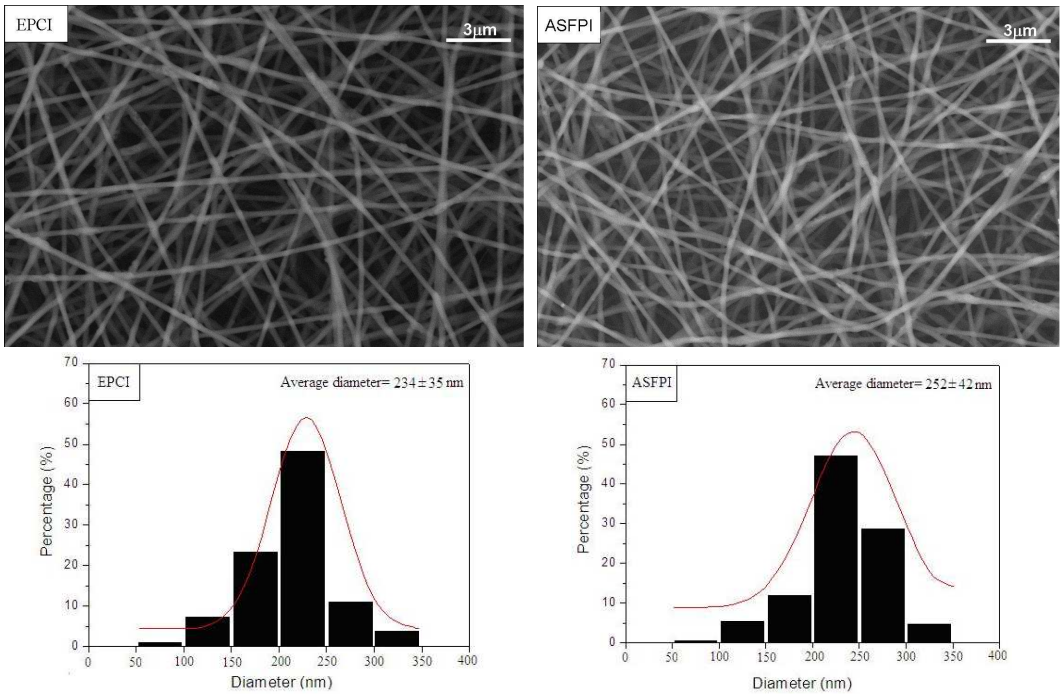

Figure 3 SEM images and fiber diameter distribution of EPCI and ASFPI nanofibers

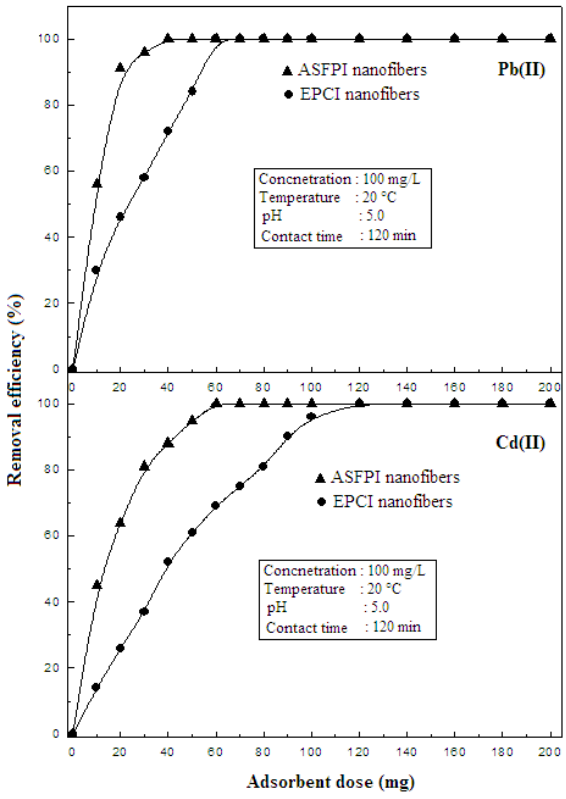

Figure 4 Effect of adsorbent dose on the removal efficiency of Pb(II) and Cd(II) by EPCI and ASFPI nanofibers

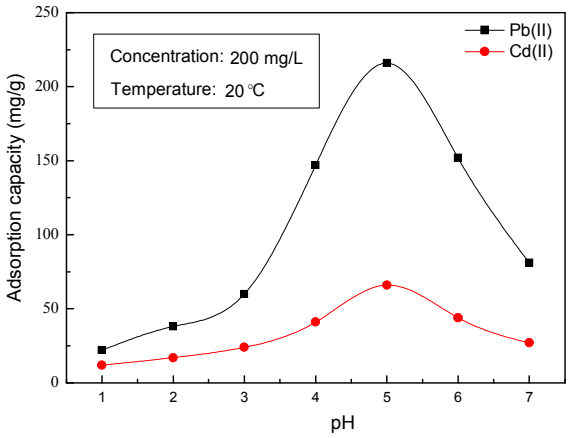

Figure 5 The effect of solution pH on Pb(II) and Cd(II) adsorption by ASFPI nanofibers

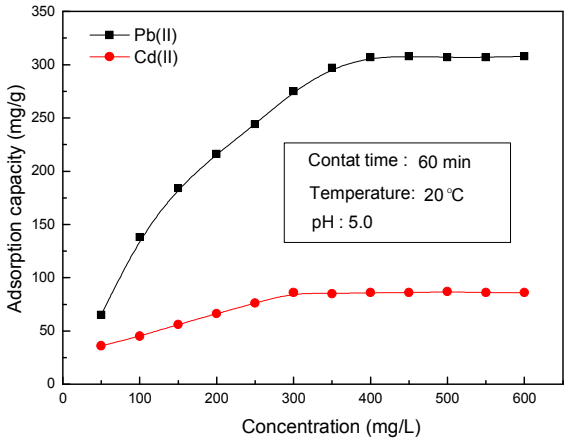

Figure 6 The effect of initial ions concentration on Pb(II) and Cd(II) adsorption by ASFPI nanofibers

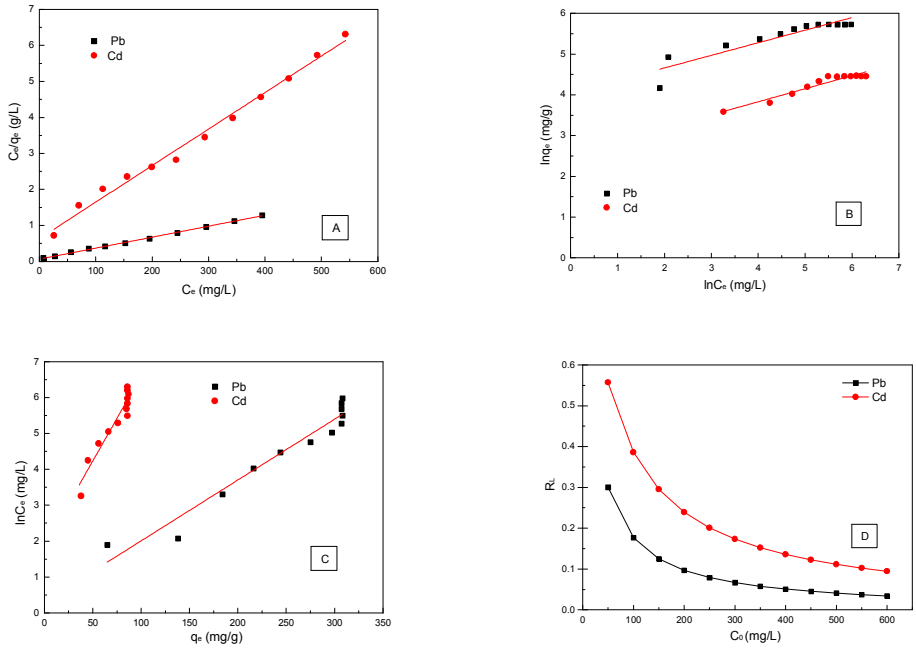

Figure 7 Sorption isotherm displayed in their linearized format and fit by the Langmuir model (A), Freundlich model (B) and Temkin model (C) and the variation of R_L with initial concentration of metal ions (D)

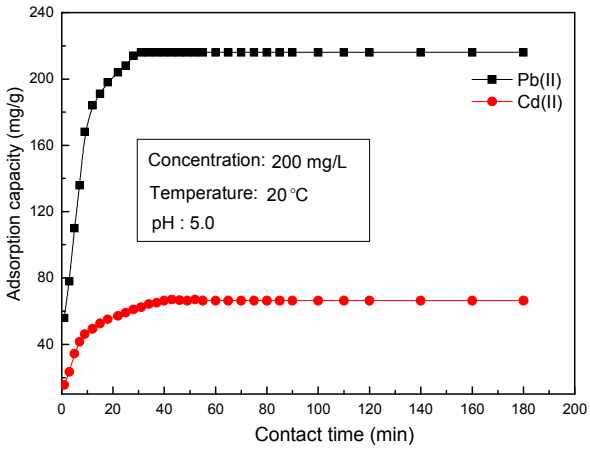

Figure 8 The effect of contact time on Pb(II) and Cd(II) adsorption by ASFPI nanofibers

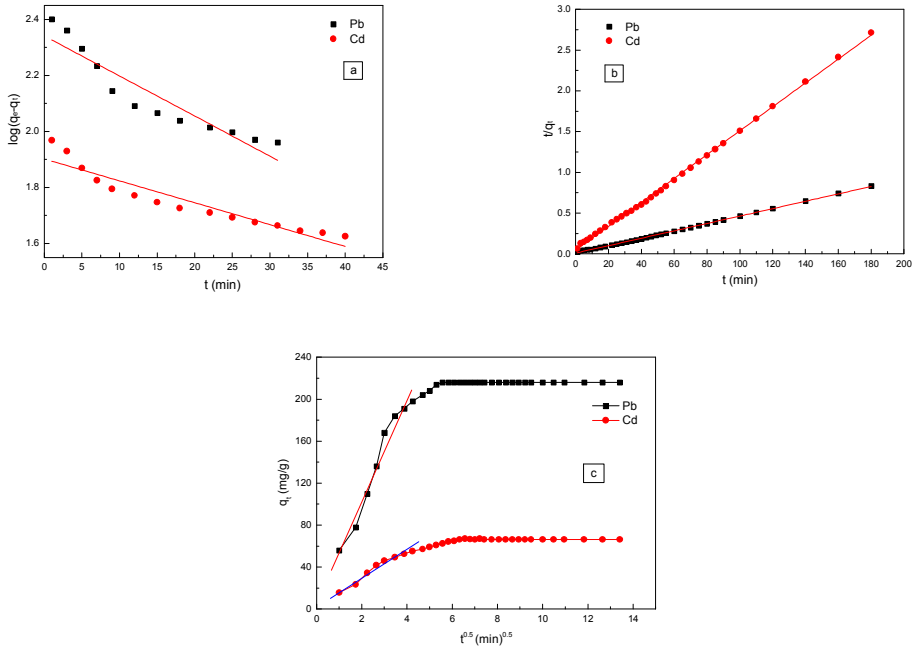

Figure 9 Data fitting for Pb(II) and Cd(II) adsorption by ASFPI nanofibers using pseudo-first-order kinetic model (a), pseudo-second-order kinetic model (b) and intra-particle diffusion model (c)

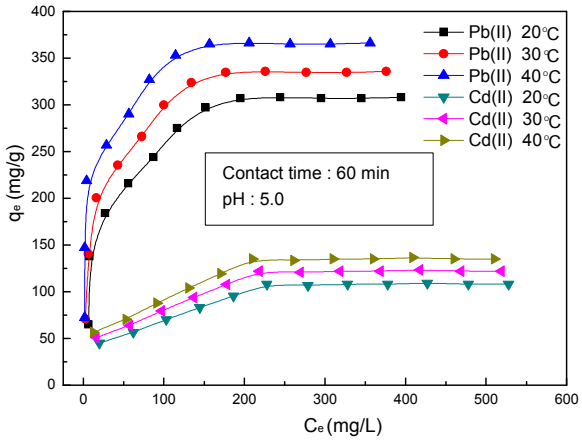

Figure 10 The effect of temperature on Pb(II) and Cd(II) adsorption by ASFPI nanofibers

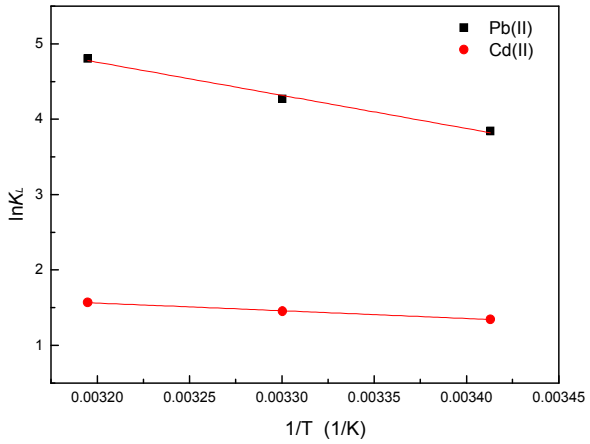

Figure 11 Plot to determine thermodynamic parameters for Pb(II) and Cd(II) adsorption by ASFPI nanofibers

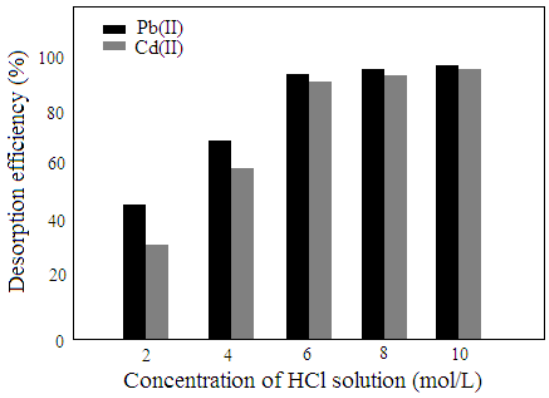

Figure 12 Desorption of Pb(II) and Cd(II) from the metal-loaded ASFPI nanofibers in HCl solution

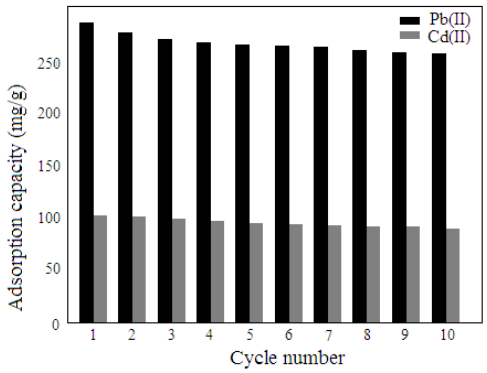

Figure 13 Adsorption capacities of ASFPI nanofibers after regeneration